BIOCHEMISTRY
including biophysical chemistry & molecular biology

Article

pubs.acs.org/biochemistry

Mycobacterium tuberculosis Utilizes a Unique Heterotetrameric Structure for Dehydrogenation of the Cholesterol Side Chain

Suzanne T. Thomas and Nicole S. Sampson*

Department of Chemistry, Stony Brook University, Stony Brook, New York 11794, United States

Supporting Information

ABSTRACT: Compounding evidence supports the important role in pathogenesis that the metabolism of cholesterol by *Mycobacterium tuberculosis* plays. Elucidating the pathway by which cholesterol is catabolized is necessary to understand the molecular mechanism by which this pathway contributes to infection. On the basis of early metabolite identification studies in multiple actinomycetes, it has been proposed that cholesterol side chain metabolism requires one or more acyl-CoA dehydrogenases (ACADs). There are 35 genes annotated as encoding ACADs in the *M. tuberculosis* genome. Here we characterize a heteromeric ACAD encoded by *Rv3544c* and *Rv3543c*, formerly named *fadE28* and *fadE29*, respectively. We now refer to genes *Rv3544c* and *Rv3543c* as *chsE1* and *chsE2*, respectively, in recognition of their validated activity in cholesterol side chain dehydrogenation. Analytical ultracentrifugation and liquid chromatography−ultraviolet experiments establish that ChsE1−ChsE2 forms an $\alpha_2\beta_2$ heterotetramer, a new architecture for an ACAD. Our bioinformatic analysis and mutagenesis studies reveal that heterotetrameric ChsE1−ChsE2 has only two active sites. E241 in ChsE2 is required for catalysis of dehydrogenation by ChsE1−ChsE2. Steady state kinetic analysis establishes the enzyme is specific for an intact steroid ring system versus hexahydroindanone substrates with specificity constants (k_{cat}/K_M) of $(2.5 \pm 0.5) \times 10^5$ s^{-1} M^{-1} versus 9.8×10^2 s^{-1} M^{-1}, respectively, at pH 8.5. The characterization of a unique ACAD quaternary structure involved in sterol metabolism that is encoded by two distinct cistronic ACAD genes opens the way to identification of additional sterol-metabolizing ACADs in *M. tuberculosis* and other actinomycetes through bioinformatic analysis.

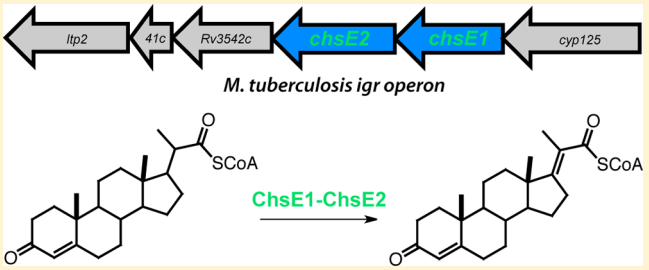

Mycobacterium tuberculosis, the causative agent of tuberculosis, is the second most deadly infection in the adult population worldwide; 8.8 million cases were reported in 2010 and 1.4 million deaths attributed to the disease.[1] During infection, *M. tuberculosis* bacilli are phagocytosed by macrophages, and the host inflammatory response results in the formation of a granuloma.[2] Bacteria can persist within the granuloma for decades.

M. tuberculosis metabolism of cholesterol, an abundant host lipid, is important for the persistence of infection *in vivo*.[3,4] Disruption of an Mce4 ABC transporter mutant results in the defective transport of cholesterol into the mycobacterium.[4,5] In infected mice, the *mce4* mutant's growth is slowed in the chronic phase of infection. *fadA5*, a cholesterol-regulated gene that encodes a thiolase, is required for the growth of *M. tuberculosis* on cholesterol as a carbon source.[6] The number of bacteria in the lungs of mice infected with the *fadA5* mutant decreased after induction of the cellular immune response, demonstrating a persistence phenotype identical to that seen upon mutation of the Mce4 transporter.[4] Thiolases catalyze the reverse Claisen condensation step in lipid β-oxidation. Similarly, the *M. tuberculosis igr* operon, which encodes six proteins, is important for growth on cholesterol *in vitro* and for mycobacterial survival *in vivo* and encodes homologues of lipid-modifying enzymes.[7,8]

The *M. tuberculosis igr* operon (*Rv3545c*−*Rv3540c*) is required for complete degradation of the cholesterol side chain. Upon disruption of this operon, steroid-derived metabolite methyl 1β-(2′-propanoate)-3aα-H-4α-(3′-propanoic acid)-7aβ-methylhexahydro-5-indanone accumulates in *M. tuberculosis* Δ*igr* cultures grown in the presence of cholesterol (Scheme 1).[9] Rv3544c and Rv3543c, annotated as potential acyl-CoA dehydrogenases, are encoded by two adjacent

Scheme 1. Methyl 1β-(2′-Propanoate)-3aα-H-4α-(3′-propanoic acid)-7aβ-methylhexahydro-5-indanone Accumulates in an *igr*-Disrupted Strain of *M. tuberculosis* when It Is Cultured with Cholesterol

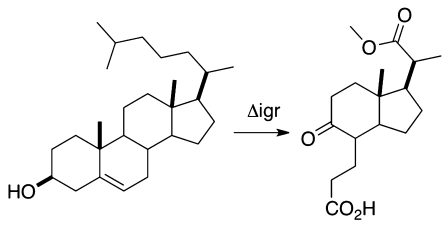

Received: March 7, 2013
Revised: April 4, 2013
Published: April 5, 2013

Table 1. Plasmids Constructed

construct name	plasmid	gene	fusion tag	restriction sites used	antibiotic marker	source or ref
	pET20b				amp	Novagen
	pET28b				kan	Novagen
	pSD31				hygro	13
	pG-KJE8				cam	Takara
pChsE1N	pET28b	*Rv3544c*	N-terminal His_6	NdeI/NotI	kan	this work
pChsE2N	pET28b	*Rv3543c*	N-terminal His_6	NdeI/XhoI	kan	this work
pChsE1	pET20b	*Rv3544c*	–	NdeI/NotI	amp	this work
pChsE2Ms	pSD31	*Rv3543c*	N-terminal His_6	EcoRv	hygro	this work
pigrS	pET28b	*Rv3544c–Rv3540c*	N-terminal His_6	NdeI/HindIII	kan	9
$pigrS_{E241Q}$	pET28b	*Rv3544c–Rv3540c*	N-terminal His_6	NdeI/HindIII	kan	this work

cistronic genes. Heterologously co-expressed N-His_6-tagged Rv3544c and tagless Rv3543c are copurified upon immobilized metal affinity chromatography, indicating they form a quaternary complex. We demonstrated that the complex is a functional acyl-CoA dehydrogenase that dehydrogenates steroid-derived substrates analogous to the metabolite isolated from an *igr* knockout strain.[9]

To the best of our knowledge, this was the first report of a heteromeric acyl-CoA dehydrogenase (ACAD). All ACADs characterized to date form homotetrameric assemblies comprised of four ~43 kDa monomers, with one exception. The ACAD subfamilies specific for very long chain fatty acids (VLCAD and ACAD9) form homodimers from two ~73 kDa monomers.[10,11]

Herein, we present a full enzymatic and biophysical characterization of Rv3543c–Rv3544c and demonstrate that Rv3543c–Rv3544c is an $\alpha_2\beta_2$ heterotetramer. Neither Rv3543c nor Rv3544c is functionally competent by itself. Extensive sequence alignments of Rv3543c and Rv3544c with acyl-CoA dehydrogenases with known three-dimensional structures reveal that a canonical active site glutamate required for general base catalysis is conserved in Rv3543c, but not in Rv3544c. Mutagenesis in combination with kinetic assays confirmed that Glu241 of Rv3543c is the base required for catalysis by this enzyme. Furthermore, Rv3543c–Rv3544c has only two conserved FAD binding sites per tetramer. Formation of the Rv3543c–Rv3544c complex is required to constitute functional binding sites and consequently catalytic activity. We propose that this unique heteromeric structure is required for effecting dehydrogenation of steroyl-CoA substrates and may be a motif that is utilized for polycyclic-CoA esters in general. Therefore, we now refer to the Rv3544c and Rv3543c acyl-CoA dehydrogenase genes as *chsE1* and *chsE2*, respectively, for cholesterol side chain metabolism E, to distinguish them from members of the bacterial *fadE*, fatty acid degradation E acyl-CoA dehydrogenase, gene family.

MATERIALS AND METHODS

Materials, Strains, Media, and General Methods. Ferricenium hexafluorophosphate and ergocalciferol were purchased from Sigma-Aldrich (St. Louis, MO). Coenzyme A was purchased from MP Biomedicals (Solon, OH). Isopropyl β-D-1-thiogalactopyranoside was from Denville Scientific (Metuchen, NJ). Tryptone, HEPES, Tris, and ampicillin were purchased from Fisher Scientific (Pittsburgh, PA). L-Arabinose, chloramphenicol, and sodium chlorite were purchased from Acros Organics. Tetracycline was from U.S. Biochemical Corp. (Cleveland, OH), and kanamycin was from IBI Scientific (Peosta, IA). Yeast extract was purchased from Research Products International Co. (Mount Prospect, IL). iProof DNA polymerase was from Bio-Rad (Hercules, CA). Restriction endonucleases, T4 DNA ligase, T4 polynucleotide kinase, and the protein ladder were from New England Biolabs (Beverly, MA). HisTrap FF columns, MonoQ, and Superdex 75 HiLoad 16/60 and 10/300 GL columns were from GE Healthcare Biosciences Corp. (Piscataway, NJ). Oligonucleotides were from IDT Inc. (Coralville, IA). Total genomic DNA of *M. tuberculosis* H37Rv was obtained from the TB Research Materials Facility at Colorado State University (Fort Collins, CO) (NIAD NO1-AI40091). MALDI mass spectra were acquired on a Bruker Autoflex II TOF/TOF instrument. Big Dye DNA sequencing (Applied Biosystems, Foster City, CA; performed by the Stony Brook University Sequencing Facility) was used to verify the coding sequence of the expression plasmids. BL21(DE3) *Escherichia coli* was obtained from Bio-Rad, and chaperone plasmid pG-KJE8 was obtained from Takara. *Mycobacterium smegmatis* strain mc^2155 was obtained from E. Dubnau (PHRI). 2× YT is composed of 16 g of tryptone, 10 g of yeast extract, and 5 g of NaCl per liter. LC–UV–MS analysis was conducted on a Waters UPLC/MS instrument with diode array and SQD detectors. Buffer A consisted of 20 mM Tris-HCl buffer (pH 8.0), supplemented with 300 mM NaCl, 1 mM TCEP, and 10 mM imidazole. Buffer B consisted of 50 mM Tris-HCl buffer (pH 8.0). Buffer C consisted of 50 mM Tris-HCl buffer (pH 8.0), supplemented with 200 mM NaCl and 1 mM TCEP. Buffer D consisted of 20 mM sodium phosphate buffer (pH 7.5), supplemented with 200 mM NaCl and 1 mM TCEP.

Expression Plasmid Construction. The desired genes were amplified from *M. tuberculosis* H37Rv total genomic DNA by polymerase chain reaction (PCR) using forward and reverse primers. The PCR product was digested with the appropriate restriction endonuclease and ligated into a similarly digested vector (Table 1). DNA sequencing of the plasmids confirmed that the sequence was correct and that no mutations were introduced during the cloning procedures. ChsE2 glutamate 241 was mutated to a glutamine in *pigrS* using the method of Moore.[12] The mutation was confirmed by DNA sequencing.

Individual Gene Expression. *pChsE1N* or *pChsE2N* constructs were transformed into BL21(DE3) *E. coli*, and single colonies were selected on LB plates containing 30 μg/mL kanamycin and cultured in 2× YT medium at 37 °C. Expression was induced at an A_{600} of 0.6–0.8 by the addition of 50 μM to 1 mM isopropyl 1-thio-β-D-galactopyranoside (IPTG), and cells were grown for 20 h at 16 or 25 °C.

Gene Expression in *M. smegmatis*. *pChsE2Ms* was electroporated into *M. smegmatis* mc^2155, and single colonies were selected on 7H10 plates supplemented with 100 μg/mL

dx.doi.org/10.1021/bi4002979 | *Biochemistry* 2013, 52, 2895–2904

ampicillin, 10 μg/mL cycloheximide, and 50 μg/mL hygromycin and grown in 7H9 medium supplemented with 0.2% glycerol. After 2 days, expression was induced with 0.2% acetamide and cultures were grown for an additional 24 h.

Gene Co-Expression. Constructs *pChsE2N* and *pChsE1* were cotransformed into BL21(DE3) *E. coli::pG-KJE8* (chaperone plasmid, Takara). Single colonies were selected on LB plates containing the appropriate antibiotics (100 μg/mL ampicillin for pET20b, 30 μg/mL kanamycin for pET28b, and 20 μg/mL chloramphenicol for pG-KJE8) and cultured in 2× YT medium at 37 °C. Chaperone expression was induced upon inoculation with 2 mg/mL L-arabinose and 5 ng/mL tetracycline. ChsE expression was induced at an A_{600} of 0.6−0.8 with the addition of 1 mM IPTG, and cells were grown for 20 h at 25 °C. Gene co-expression *in cis* with construct *pigr5* was performed as reported previously.[9] Similarly, the $ChsE2_{E241Q}$ mutant protein was prepared with construct $pigr5_{E241Q}$ using the expression conditions that were used for *pigr5*.

Protein Purification. ChsE1- or ChsE2-expressing cells were lysed with a French press in buffer A, and cellular debris was removed by centrifugation at 125000*g* for 1 h. Proteins were purified by immobilized metal affinity chromatography using Hisbind resin (Novagen) following the manufacturer's protocol. Soluble ChsE2 was buffer exchanged with buffer B and further purified by anion exchange chromatography on a MonoQ column (1 mL) equilibrated in buffer B. Protein was eluted at a flow rate of 0.5 mL/min with a linear gradient from 100 to 100% buffer B supplemented with 1 M NaCl. After injection, the column was washed with 5 column volumes (CV) of buffer B, which was then changed to 80% buffer B over 20 CV. Next, the gradient was changed from 80 to 25% buffer B over 10 CV and then to 0% buffer B over 5 CV. Eluted protein was further purified by size exclusion chromatography on a Superdex 200 HiLoad 16/60 column (GE Healthcare) equilibrated with buffer C. ChsE1−ChsE2 and ChsE1−$ChsE2_{E241Q}$ were purified as detailed for ChsE2, excluding the anion exchange chromatography step. All protein samples were analyzed by reducing sodium dodecyl sulfate−polyacrylamide gel electrophoresis (SDS−PAGE), and protein band identities were confirmed by in-gel tryptic digestion as reported previously.[14] ChsE proteins were stored in 50 mM HEPES buffer (pH 8.0) at −80 °C.

Identification and Quantification of a Flavin Cofactor. A 15 μM (1.2 mg/mL) solution of ChsE1−ChsE2 in buffer C was denatured by being boiled for 2 min. The sample was chilled on ice and centrifuged to pellet precipitated protein. The supernatant was analyzed by reverse phase C18 liquid chromatography−mass spectrometry in ESI positive mode and compared to the flavin adenine dinucleotide standard. The quantity of FAD obtained was determined using the absorbance and extinction coefficient of FAD at 260 nm (ε_{260} = 37000 M^{-1} cm^{-1}). The protein pellet was dissolved in 6 M guanidine hydrochloride and the concentration determined using the calculated extinction coefficients at 280 nm: ε_{280}(ChsE1) = 35410 M^{-1} cm^{-1}, ε_{280}(ChsE2) = 58900 M^{-1} cm^{-1}, and ε_{280}(ChsE1−ChsE2) = 188620 M^{-1} cm^{-1}.

Biophysical Analysis of ChsE Proteins. ChsE2, ChsE1−ChsE2, and ChsE1−$ChsE2_{E241Q}$ samples were analyzed by analytical gel filtration on a Superdex 75 10/300 GL column (GE Healthcare) equilibrated with buffer D. Samples were eluted isocratically in the same buffer, monitoring at 220 and 280 nm.

Molecular masses of ChsE2 and ChsE1−ChsE2 were determined using analytical ultracentrifugation sedimentation equilibrium with a Beckman Optima XL-A centrifuge. ChsE2 (8.5, 3.4, and 1.7 μM) in 5 mM sodium phosphate buffer (pH 7.5) and ChsE1−ChsE2 (10.6, 5.3, and 2.6 μM) in buffer B were centrifuged at 20K, 25K, and 30K rpm and 20 °C. Scans were acquired after centrifugation for 18 and 20 h at each speed by monitoring at 280 nm. The protein partial-specific volumes of 0.7336 for ChsE2 and 0.7350 for ChsE1−ChsE2 and the solvent densities of 0.9994 for ChsE2 and 1.0079 for ChsE1−ChsE2 were calculated using SEDNTERP (University of New Hampshire, Durham, NH). Data were fit globally to the ideal, single-species model using Heteroanalysis (University of Connecticut, Storrs, CT) to determine the molecular mass.

The protein complex stoichiometry of ChsE1−ChsE2 was confirmed by LC−UV−MS (Waters UPLC/diode array/SQD). ChsE1 and ChsE2 were separated on a Waters XBridge BEH300 C4 3.5 μm column (2.1 mm × 100 mm) at 40 °C with a linear gradient from 95% A to 95% B over 15 min, where A consists of 5% 2-propanol and 0.1% trifluoroacetic acid and B consists of 99.9% 2-propanol and 0.1% trifluoroacetic acid. MS spectra were collected in ESI positive ion mode with a cone voltage of 40 V, a capillary voltage of 4.5 kV, and a source temperature of 150 °C. MS spectra were deconvolved using ESIprot version 1.0,[15] and peaks in the UV 280 nm chromatograms were integrated using R. The integrated peak areas of each protein were divided by the corresponding molar extinction coefficient for the protein to yield the molar concentrations. The protein stoichiometry was determined from the ratio of the molar concentrations.

Bioinformatic Analysis. ACAD protein sequences were obtained from UniProt, and sequence alignments were conducted with ClustalW2 (EMBL-EBI, European Bioinformatics Institute, Cambridge, U.K.) using the default parameters.[16] FAD binding and CoA binding in published ACAD Protein Data Bank (PPDB) structures were investigated with PoseView (Center of Bioinformatics, University of Hamburg, Hamburg, Germany).[17] A ChsE1−ChsE2 ligand binding model was created using the MCAD homodimer (PDB entry 1EGC) as a template. The model is based on a ChsE1−ChsE2 heterodimer assembly and highlights conserved residues determined from the ACAD sequence alignment with ChsE1 and ChsE2.

Dehydrogenase Assay. CoA thioesters, 3-oxo-4-pregnene-20-carboxyl-CoA (**1**) and 1β-(2′-propanoyl-CoA)-3aα-H-7aβ-methylhexahydro-4-indanone (**2**), were prepared and purified as reported previously.[9,18] The identities and purity of CoA thioesters were assessed by LC−UV−MS.

Dehydrogenase activity was tested with artificial electron acceptor ferricenium hexafluorophosphate as reported previously.[19] Product formation was monitored spectroscopically at 300 nm and 25 °C. Initial velocities were determined for the first 100 s of the reaction. Enzyme activity was optimized for pH using the three component buffer system reported by Ellis and Morrison with 50 μM acyl-CoA **1**.[20] Subsequent assays were conducted in 100 mM TAPS buffer (pH 8.5). The optimal ionic strength was investigated at NaCl concentrations from 0 to 1.0 M. Protein stability and substrate **1** solubility were tested at concentrations of 100 nM and 50 μM, respectively, with and without 0.2 M NaCl by dynamic light scattering on a 90 Plus particle size analyzer from Brookhaven Instruments Corp. Data were acquired in triplicate at 25 °C.

dx.doi.org/10.1021/bi4002979 | *Biochemistry* 2013, 52, 2895−2904

Steady state kinetic analysis was conducted in 100 mM TAPS buffer (pH 8.5) with CoA thioesters **1** and **2**. The rates of product formation were fit to the Michaelis–Menten equation (eq 1) to determine the K_M values for substrates **1** and **2** and the k_{cat} for enoyl-CoA product formation.

$$v = V_{max}[S]/(K_M + [S]) \quad (1)$$

where v is the initial velocity, V_{max} is the maximal velocity, S is the varied substrate, and K_M is the Michaelis–Menten constant.

NMR Analysis of the Assay Product. The product of the ChsE1–ChsE2 assay with substrate 3-oxo-4-pregnene-20-carboxyl-CoA was purified on a 3 cc sep-pak C18 cartridge (Waters) equilibrated in a 5% MeOH/95% 10 mM ammonium acetate mixture (pH 8.0). After the sample had been loaded, the cartridge was washed with 6 mL of equilibration buffer followed by 6 mL of a 25% MeOH/75% 10 mM ammonium acetate mixture (pH 8.0). The product was eluted in a 45% MeOH/55% 10 mM ammonium acetate mixture (pH 8.0). The dried compound was dissolved in D_2O for NMR analysis on a Bruker 700 MHz NMR instrument. ^{1}H NMR spectra of substrate **1** and the purified product were acquired using excitation sculpting for water suppression.[21]

RESULTS

ChsE2 Is Isolated as a Monomeric Apoenzyme When Heterologously Expressed in either *E. coli* or *M. smegmatis*. Initially, *chsE1* and *chsE2* were expressed individually in *E. coli* as N-terminally His_6-tagged proteins. ChsE1 was found to be insoluble and was localized in inclusion bodies. ChsE2 was isolated and purified by immobilized metal affinity, anion exchange, and size exclusion chromatographies (Figure S1 of the Supporting Information). UV–visible spectroscopy revealed the protein was purified as the apoprotein, without the flavin cofactor necessary for catalysis (Figure 1). Attempts to reconstitute the protein with FAD were not successful.

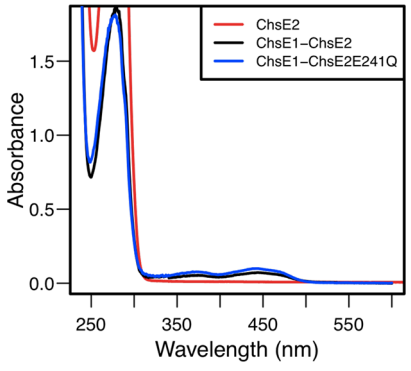

Figure 1. UV–visible spectra of purified ChsE2 (50 μM), ChsE1–ChsE2 (15 μM), and ChsE1–$ChsE2_{E241Q}$ (15 μM). Relative spectral maxima at 370 and 446 nm for ChsE1–ChsE2 and ChsE1–$ChsE2_{E241Q}$ are characteristic of oxidized flavin. No flavin absorbance was observed for ChsE2 alone.

ChsE2 was analyzed by analytical size exclusion chromatography (Figure 2) and analytical ultracentrifugation (AUC) sedimentation equilibrium experiments (Figure 3A). The predicted monomer molecular mass with a His_6 tag is 44.9 kDa. The AUC data fit an ideal model with a molecular mass of 42.0 ± 0.5 kDa, where the reported error is the measure of the fit and indicates the chosen model is satisfactory. Thus, under

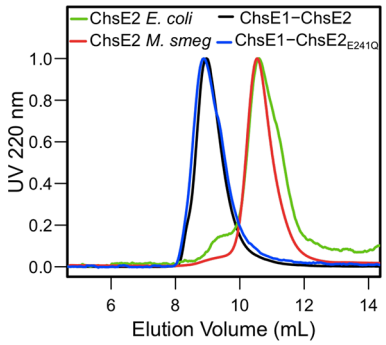

Figure 2. Analytical gel filtration of ChsE2 and ChsE1–ChsE2 complexes. ChsE2 expressed in *E. coli* and *M. smegmatis* and ChsE1–ChsE2 and ChsE1–$ChsE2_{E241Q}$ expressed in *E. coli* were analyzed by analytical gel filtration on a Superdex 75 column under identical conditions. The signal at 220 nm was normalized to 1.0. The ChsE1–ChsE2 protein formed a stable complex with a molecular mass higher than that of ChsE2 expressed alone in *E. coli* or *M. smegmatis*.

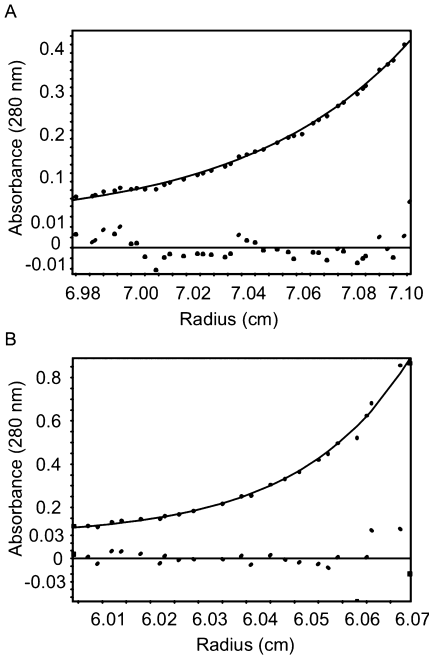

Figure 3. Analytical ultracentrifugation sedimentation equilibrium data for ChsE proteins. (A) ChsE2 and (B) ChsE1–ChsE2 were analyzed at three concentrations ranging from 1 to 11 μM at centrifugation speeds of 20K, 25K, and 30K rpm at 20 °C. A representative fit for each sample is shown. The solid line shows the fit of the data to the ideal species model, and the residuals of the fit are graphed below. The global fit for each protein provided molecular masses of 42.0 ± 0.5 and 156 ± 1 kDa for ChsE2 and ChsE1–ChsE2, respectively.

the conditions tested, ChsE2 is a monomer. In crystal structures of ACADs, one molecule of FAD binds non-covalently per monomer and the adenosine lies at the interface of the two monomers. Therefore, two monomer chains comprise the FAD binding pocket, and ChsE2 may not bind FAD because of its monomeric state.

Next, *chsE2* was expressed in *M. smegmatis*, a nonpathogenic, faster-growing relative of *M. tuberculosis*, as an N-terminally His_6-tagged protein. The protein was isolated by immobilized metal affinity chromatography (IMAC) and further purified by anion exchange and size exclusion chromatographies. Analysis by analytical size exclusion chromatography indicated that *M.*

dx.doi.org/10.1021/bi4002979 | *Biochemistry* 2013, 52, 2895–2904

smegmatis expressed ChsE2 was also monomeric (Figure 2). Analysis of ChsE2 expressed in *E. coli* and in *M. smegmatis* demonstrates that the protein is not in the predicted quaternary structure of ACADs, lacks FAD, and therefore is inactive.

The ChsE1−ChsE2 Complex Forms an Obligate $\alpha_2\beta_2$ Tetramer with Noncovalently Bound FAD. Isolation of monomeric ChsE2 apoprotein and insoluble ChsE1 indicated they do not form native structures as individual proteins. Previously, we had reasoned that these proteins might form a complex because they are encoded in a single operon. Co-expression would allow assembly of ChsE1 and ChsE2 that would otherwise be insoluble or inactive when expressed individually. Indeed, when *chsE1* and *chsE2* were expressed in a cistronic construct on a single plasmid, *pigr5*, a complex of ChsE1 and ChsE2 was isolated in a pull-down assay.[9]

Here, we further investigated expression conditions and constructs. We found that the ChsE1−ChsE2 complex was obtained upon expressing *chsE1* as a tagless protein and *chsE2* as an N-terminally His_6-tagged protein from separate plasmids (*in trans*) in *E. coli* with co-expression of chaperones. We used *E. coli* harboring plasmid pG-KJE8, which encodes five folding chaperones, DnaK, DnaJ, GrpE, GroES, and GroEL. The ChsE1−ChsE2 protein complex was isolated regardless of which protein, ChsE1 or ChsE2, contained an N-terminal His_6 tag. The identity of ChsE1 and ChsE2 in the complex was confirmed by SDS−PAGE (Figure S1 of the Supporting Information) and in-gel tryptic digest followed by MALDI-TOF MS analysis.

Under both *in cis* and *in trans* expression conditions, the isolated complex was yellow in appearance and had a characteristic UV−visible flavin spectrum, with absorbance maxima at 370 and 446 nm (Figure 1). Expression *in cis*, however, yielded higher A_{446}/A_{280} ratios, indicative of higher FAD occupancy. Kinetic studies were conducted with ChsE1−ChsE2 expressed with construct *pigr5*.

The flavin cofactor was released from ChsE1−ChsE2 by heat denaturation of the protein and was analyzed by LC−UV−MS. A protonated molecular ion at m/z 786 was observed (Figure S2 of the Supporting Information), confirming the identity of the cofactor as FAD. In addition, the retention time and absorbance spectrum were identical to those of a FAD standard. Therefore, ChsE1−ChsE2 is isolated as a holoprotein with the FAD cofactor.

Analysis of the complex by analytical size exclusion chromatography confirmed that a stable quaternary complex is formed (Figure 2). Further analysis by AUC sedimentation equilibrium experiments established that ChsE1−ChsE2 exists as a tetramer with a molecular mass of 156 ± 1 kDa (Figure 3B). The predicted molecular masses of N-tagged ChsE1 and ChsE2 are 37.6 and 42.7 kDa, respectively. To determine precisely the stoichiometry of the complex, the assembly was analyzed by LC−UV−MS (Figure 4). The two observed peaks were identified as ChsE1 and ChsE2 by ESI+ MS. The absorbance peaks at 280 nm for ChsE1 and ChsE2 were integrated, and using the extinction coefficient for each protein, the relative molar stoichiometry of ChsE1 to ChsE2 was calculated to be 1:1. This ratio indicates that the ChsE1−ChsE2 species forms an $\alpha_2\beta_2$ complex.

The Tetrameric ChsE1−ChsE2 Complex Has Two Cofactor Binding Sites. The FAD stoichiometry in the protein complex was determined spectrophotometrically after protein denaturation. The protein concentration was determined for the unfolded protein using the calculated extinction

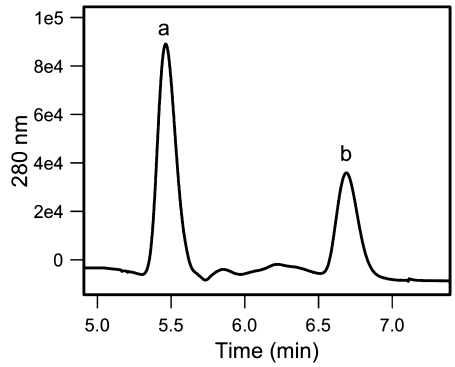

Figure 4. Reverse phase LC−UV chromatogram of ChsE1−ChsE2. Peak a and peak b were identified as ChsE2 and ChsE1, respectively, by deconvolution of multiple charged states in the corresponding ESI+ MS spectra. The absorbance peaks were integrated and relative concentrations determined from the calculated extinction coefficients of ChsE1 and ChsE2 [ε_{280}(ChsE1) = 35410 M^{-1} cm^{-1}, and ε_{280}(ChsE2) = 58900 M^{-1} cm^{-1}].

coefficient of ChsE1 and ChsE2 at 280 nm. The concentration of FAD was calculated from the extinction coefficient at 260 nm after removal of precipitated ChsE1−ChsE2. The FAD:protein molar ratio was 1.4 ± 0.1 FAD molecules per $\alpha_2\beta_2$ ChsE1−ChsE2 tetramer. This result suggests that ChsE1−ChsE2 has two FAD bindings sites in contrast to typical ACAD tetramers that have four FAD binding sites.

To corroborate the FAD stoichiometry in heterotetrameric ChsE1−ChsE2, we analyzed the protein sequences of ChsE1 and ChsE2 for FAD binding residues that are conserved in other ACADs. First, we examined ligand−protein interactions between FAD and several ACADs in reported crystal structures (PDB entry in parentheses), including human SCAD (2VIG), MCAD (1EGC), SBCAD (2JIF), IBD (1RX0), IVD (1IVH), GD (1SIQ), VLCAD (3B96), and ACAD11 (2WBI) and bacterial ACADS from *Megsphaera elsdenii* (1BUC) and *Mycobacterium thermoresistibile* (3NF4). In each structure, a single FAD cofactor binding site is comprised of two chains from the ACAD tetramer or dimer, in the case of VLCAD and ACAD9. Each chain interacts with adenosine in one binding pocket and with riboflavin in a second binding pocket. The polar side chains of Thr161A, Ser167A, Thr193A, and Thr403A form hydrogen bonds with the isoalloxazine and ribityl diphosphate moieties (numbering from MCAD). These Ser and Thr residues are conserved within the ACAD family (Figure 5A).

Analysis of the ChsE2 and ChsE1 sequence alignments with these ACADs revealed that Thr161A, Ser167A, and Thr193A are conserved in ChsE2 as residues Thr126, Thr132, and Thr158, respectively. Thr403A is not conserved in ChsE2 (Figure 5A). In contrast, Thr161A, Ser167A, Thr193A, and Thr403A are not conserved in ChsE1.

Residues involved in forming hydrogen bonds with adenosine of FAD, Arg306A′, Gln317A′, Gln374A′, and Gly378A′, are from the second chain that contributes to the FAD cofactor binding sites in ACADs and are highly conserved. Sequence analysis of ChsE1 revealed that Arg306A′, Gln317A′, Gln374A′, and Gly378A′ align with residues Arg227, Gln238, His295, and Gly299, respectively (Figure 5A). However, Arg306A′, Gln317A′, Gln374A′, and Gly378A′ are not conserved in ChsE2.

dx.doi.org/10.1021/bi4002979 | *Biochemistry* 2013, 52, 2895−2904

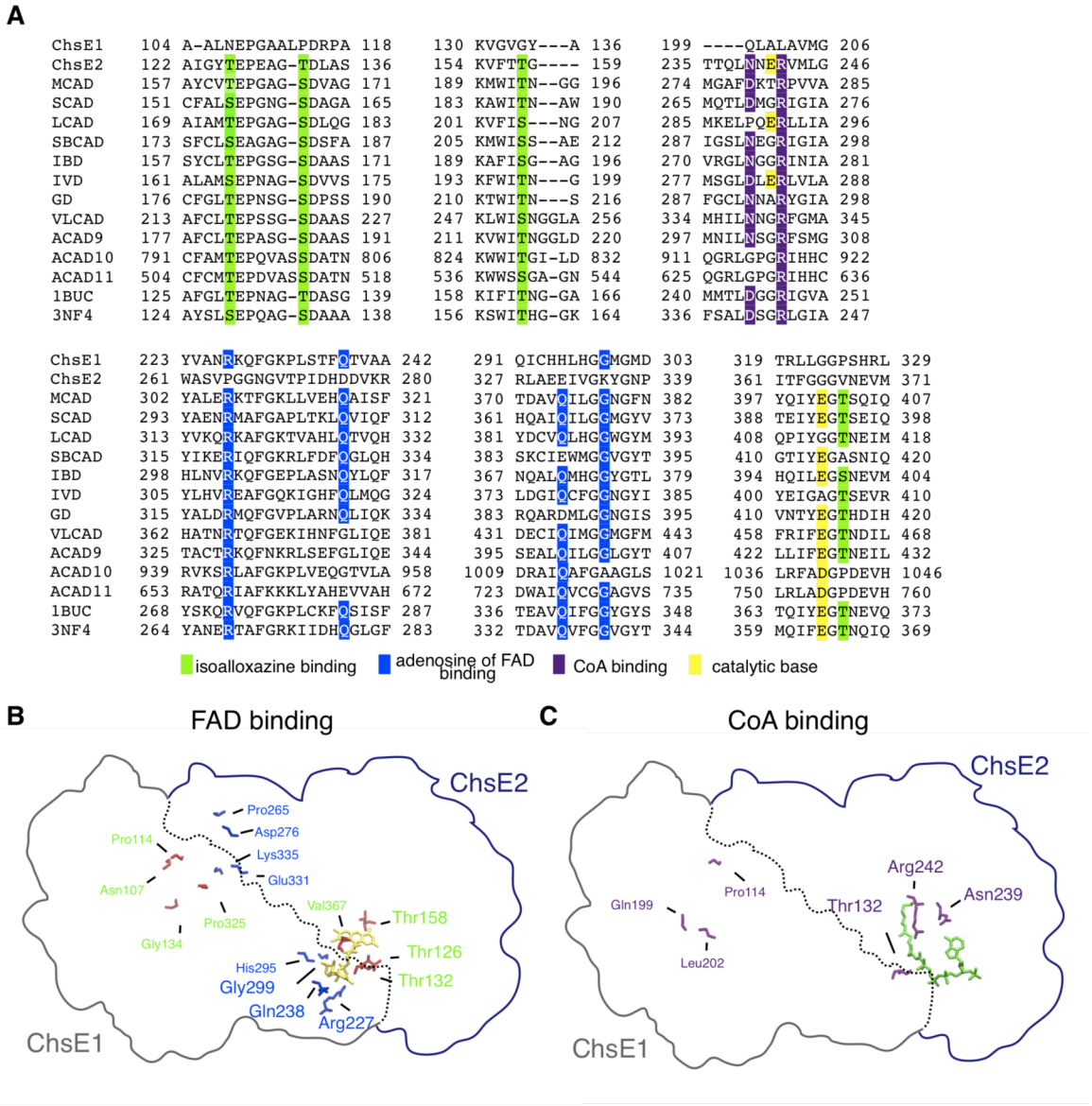

Figure 5. Bioinformatic analysis of ChsE1 and ChsE2. (A) Sequence alignment of ChsE1 and ChsE2 against human and bacterial ACADS: MCAD (P11310), SCAD (P16219), LCAD (P28330), SBCAD (P45954), iBD (Q9UKU7), IVD (P26440), GD (Q92947), VLCAD (P49748), ACAD9 (Q9H845), ACAD10 (Q6JQN1), ACAD11 (Q709F0), 1BUC (SCAD *Mg. elsdenii*, Q06319), and 3NF4 (*M. thermoresistibile*, G7CDN2). Residues highlighted in green bind the isoalloxazine and ribityl diphosphate moieties of FAD. Residues highlighted in blue bind adenosine of FAD. Residues highlighted in purple bind CoA. Residues highlighted in yellow are the catalytic bases. (B) Homology model of FAD binding residues and (C) octanoyl-CoA binding residues in ChsE1−ChsE2 based on the human MCAD homodimer (PDB entry 1EGC). FAD is colored yellow and octanoyl-CoA green. FAD and CoA cofactors are shown adjacent to conserved binding residues.

In all ACAD crystal structures determined to date, two FAD cofactors bind at each dimer interface. In contrast, only one set of FAD binding site residues is conserved in the homology model of the ChsE1−ChsE2 interface. The lack of conserved riboflavin binding residues in ChsE1 and adenosine binding residues in ChsE2 indicates that one FAD cofactor binds at the ChsE1−ChsE2 heterodimer interface (Figure 5B), and that two heterodimeric units comprise the heterotetramer. This homology model is consistent with the experimentally determined FAD stoichiometry for ChsE1−ChsE2. Isolation of monomeric apo-ChsE2 suggests it does not self-associate to form a homodimer and further supports our model.

Tetrameric ChsE1−ChsE2 Has Two Active Sites. The FAD binding stoichiometry and binding residue conservation in tetrameric ChsE1−ChsE2 suggest that the complex has two active sites. ACADs require a catalytic base for activity, and this base is highly conserved in the ACAD protein family (Figure 5A). The catalytic base is most often a glutamate and is located at one of two positions in helix G or helices J and K.[22] Glutamate at either of these two positions orients in the active site in a catalytically competent configuration in the three-dimensional protein structures of ACADs.

In the ChsE2 sequence alignment with representative ACAD family members, Glu241 aligns with the glutamate of IVD and LCAD in helix G (Figure 5A). There is not a conserved glutamate in the alignment of helices J and K with ChsE2. Notably, ChsE1 does not have a glutamate or aspartate that aligns with either helix G or helices J and K. The conserved glutamates in helix G and helices J and K align with glycine residues in ChsE1. The lack of a potential active site base, in

dx.doi.org/10.1021/bi4002979 | *Biochemistry* 2013, 52, 2895−2904

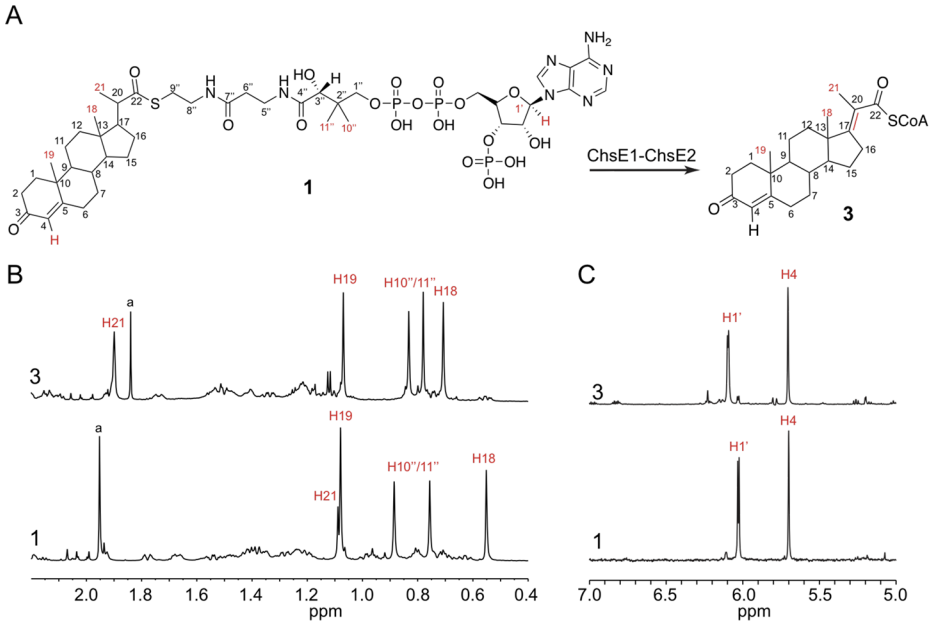

Figure 6. Characterization of the dehydrogenated product by ChsE1−ChsE2. ^{1}H NMR spectra (700 MHz) of substrate **1** and ChsE1−ChsE2 assay product **3** illustrating the changes in the methyl (B) and alkene (C) regions. The alkene stereochemistry is represented as *E* but was not determined.

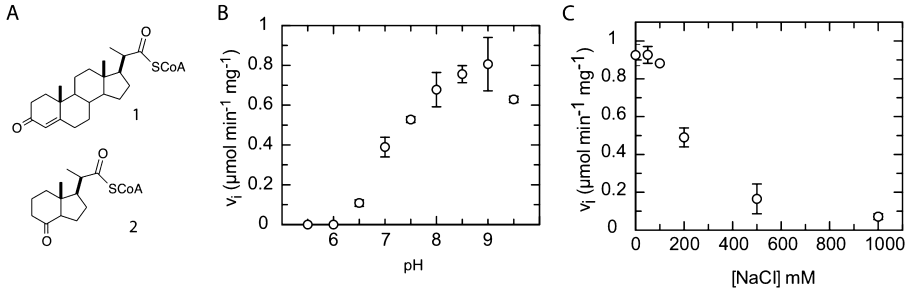

Figure 7. Optimization of dehydrogenase activity of ChsE1−ChsE2. (A) 3-Oxo-4-pregnene-20-carboxyl-CoA **1** and 1β-(2′-propanoyl-CoA)-3aα-H-7aβ-methylhexahydro-4-indanone **2**, substrates of ChsE1−ChsE2. (B) pH and (C) ionic strength optimization of dehydrogenase activity. Assays were conducted with 50 μM substrate **1** and 250 μM ferricenium hexafluorophosphate at 25 °C. Assays used to produce the data in panel C were conducted in 100 mM TAPS buffer (pH 8.5).

addition to the lack of riboflavin binding residues in ChsE1, suggests that ChsE1−ChsE2 has only two active sites, in contrast to traditional homotetrameric ACADs, which have four active sites. On the basis of these alignments, we hypothesized that Glu241 of ChsE2 is the catalytic base responsible for deprotonation during catalysis.

Analysis of the CoA binding site in the three-dimensional structures of ACADs identified conserved CoA hydrogen-bonding residues Ser142A, Arg256A, and Asp253A (numbering for human MCAD). The side chain of Arg256 forms a hydrogen bond network with the pantetheine group of CoA and is highly conserved in the ACAD family. Arg256 is conserved in ChsE2 as Arg242. In ChsE1, Leu202 aligns with Arg256. Asp253 in MCAD forms a hydrogen bond with the adenine moiety of CoA. In GD and IBD, however, this residue is an Asn, and analysis of the crystallographic structure shows the backbone carbonyl of Asn forms a hydrogen bond with adenine. Asn is conserved in ChsE2 as residue Asn239, and this residue is Val204 in ChsE1. The lack of CoA binding residues in ChsE1 supports our hypothesis that ChsE1 is not an active homtetrameric ACAD.

The ChsE1−ChsE2 Complex Forms 3-Oxo-pregna-4,17-dien-20-carboxyl-CoA (3). ^{1}H NMR spectra of substrate **1** and product **3** were acquired in D_2O (Figure 6). Comparison of substrate and product ^{1}H NMR spectra highlights the disappearance of the coupling of the C21 methyl hydrogen to H21 (δ 1.09, d). The C21 methyl becomes a singlet at 1.84 ppm (Figure 6B). If C20−C21 bond dehydrogenation had occurred, two new alkene protons would have replaced the C21 methyl in the product spectrum. However, a new proton resonance in the alkene region was not observed (Figure 6C). We conclude that the ChsE1−ChsE2 complex forms the thermodynamically favored tetrasubstituted alkene product **3**.

Steady State Kinetics of ChsE1−ChsE2. Previously, we had demonstrated that the pregnene-carboxyl-CoA ester (**1**) and indanone CoA ester (**2**) are substrates of ChsE1−ChsE2 (Figure 7A). Here, we determine the pH and ionic strength dependence of ChsE1−ChsE2. Initial velocity data were collected for ChsE1−ChsE2 with substrate **1** from pH 5.5 to 9.5 in 0.5 pH unit steps. No activity was observed at pH ≤6.0, and the highest activity was observed at pH >8.0 (Figure 7B). Further experiments were conducted at pH 8.5 in TAPS buffer.

The ChsE1−ChsE2 complex was then assayed as a function of NaCl concentration to determine the optimal ionic strength (Figure 6C). Initial velocities were determined at NaCl

dx.doi.org/10.1021/bi4002979 | *Biochemistry* 2013, 52, 2895−2904

concentrations from 0 to 1.0 M with 50 μM substrate **1**. Increasing the ionic strength by addition of NaCl diminished activity, and no rate enhancement was observed even at low concentrations of NaCl. We tested the protein stability and substrate solubility at working concentrations using dynamic light scattering at 0 and 0.2 M NaCl. The activity of ChsE1−ChsE2 was reduced by 50% in 0.2 M NaCl. However, neither protein aggregation nor substrate precipitation was observed. The decrease in enzyme activity is not due to protein denaturation or substrate aggregation.

Next, the ionic strength was increased with halide salts KCl, $MgCl_2$, $CaCl_2$, NaI, and NaBr, as well as sodium acetate (Figure S3 of the Supporting Information). The specific activity was reduced in the presence of all the tested salts. Further analysis would be required to determine the cause of rate reduction.

Steady state kinetic constants K_M and k_{cat} were determined for CoA thioesters **1** and **2** under the optimized assay conditions of 100 mM TAPS, pH 8.5, and 25 °C with 250 μM ferricenium hexafluorophosphate (Table 2). Assays were initiated by the addition of ChsE1−ChsE2, and initial velocities were determined at substrate concentrations from 0 to 200 μM, following the reduction of electron acceptor ferricenium hexafluorophosphate at 300 nm. Controls without enzyme or without substrate showed negligible decreases in absorbance at 300 nm. The calculated specificity constants (k_{cat}/K_M) indicate that the four-ring steroid **1** is the preferred substrate of ChsE1−ChSE2 relative to the 2-ring hexahydroindanone substrate **2**.

Table 2. Michaelis−Menten Kinetic Constants for ChsE1−ChsE2[a]

substrate	K_M (μM)	k_{cat} (min^{-1})	k_{cat}/K_M (s^{-1} M^{-1})
1	5.3 ± 0.9	78 ± 1	(2.5 ± 0.5) × 10^5
2	86 ± 7	5.1 ± 0.2	(9.8 ± 0.8) × 10^2

[a]The ChsE1−ChsE2 complex was assayed with CoA thioesters **1** and **2** in 100 mM TAPS buffer (pH 8.5) with 250 μM ferricenium hexafluorophosphate at 25 °C. Three independent replicates were performed. The errors are the standard deviations of the fit.

Glutamate 241 of ChsE2 Is Required for the Dehydrogenase Activity of ChsE1−ChsE2. To experimentally demonstrate that ChsE2 Glu241 is the active site base of ChsE1−ChsE2, glutamate 241 of ChsE2 was mutated to a glutamine in *pigr5*. The purified mutant protein showed characteristic flavin absorbances by UV−visible spectroscopy (Figure 1). ChsE1−$ChsE2_{E241Q}$ was analyzed by SDS−PAGE (Figure S1 of the Supporting Information) and analytical size exclusion chromatography (Figure 2), under conditions identical to those used for ChsE1−ChsE2. The elution profiles of the mutant and wild-type protein were identical, indicating that ChsE1−$ChsE2_{E241Q}$ forms an $\alpha_2\beta_2$ heterotetramer like ChsE1−ChsE2. The activity of ChsE1−$ChsE2_{E241Q}$ was tested under the optimized steady state conditions at pH 8.5 in TAPS buffer with substrate **1**. No detectable turnover was observed at concentrations of 5 μM ChsE1-$ChsE2_{E241Q}$ and 200 μM substrate **1**.

DISCUSSION

Sterol metabolism by actinomycetes has been extensively studied. However, little is known about the genes required for the β-oxidation of the sterol side chain. Partially metabolized cholesterol side chain intermediates in Nocardia established that cholesterol side chain metabolism proceeds through C24 and C22 intermediates, presumably via two rounds of conventional fatty acid β-oxidation.[23−25] The mechanism of the final loss of propionate has not been established. We previously showed through metabolite characterization in a *M. tuberculosis igr* knockout strain cultured with cholesterol that the *igr* operon is required for the complete metabolism of the cholesterol side chain.[9] The enzymes encoded by the *igr* operon are likely responsible for the final loss of propionate, resulting in full side chain metabolism. Here we characterize a cholesterol side chain degrading ACAD, ChsE1−ChsE2, encoded by the *M. tuberculosis igr* operon.

ACADs have been identified in plants,[26] animals, bacteria, nematodes,[27] and fungi.[28] The family of enzymes has been extensively studied in eukaryotes.[29] There are 11 eukaryotic classes of ACADs that vary in their substrate specificities. Seven classes are involved in fatty acid metabolism, and the four remaining classes are involved in leucine, isoleucine, valine, lysine, and tryptophan metabolism. Prokaryotic ACADs, also known as fatty acid-degrading E (FadE) enzymes, characterized to date have less distinct substrate specificities than eukaryotic ACADs and have not been categorized into distinct classes.[30,31] However, eukaryotic and bacterial ACAD sequences are highly homologous and typically align well with the eukaryotic ACADs.[32]

Our biophysical analysis demonstrates that ChsE1−ChsE2 forms an $\alpha_2\beta_2$ heterotetramer, a unique quaternary structure for an ACAD. Typical ACADs form homotetramers with the exception of the very long chain classes of ACADs that form homodimers and have an 180 additional C-terminal residues that bind to the mitochondrial membrane.[10,33]

Bioinformatics analysis and mutagenesis results demonstrate that the heteromeric ChsE1−ChsE2 complex has two FAD binding sites and two active sites, unlike traditional tetrameric ACADs with four active sites, one per subunit. Formation of the ChsE1−ChsE2 complex is necessary for FAD binding. *chsE2* expressed in the absence of *chsE1* yields monomeric ChsE2 without FAD bound. Bioinformatics analysis shows that neither ChsE1 nor ChsE2 has a complete FAD binding site and both chains are required for FAD binding. This analysis further supports the necessity of heteromeric complex formation for forming active protein. The ChsE1−ChsE2 complex from *M. tuberculosis* represents a third quaternary architecture for ACADs, in which a heterotetrameric ACAD enzyme has two active sites.

The evolution of the ACAD family is highly dynamic, and members have evolved to accommodate a variety of substrates by increasing the binding pocket size.[32,34] Highly conserved residues, like the catalytic glutamate, are usually evolutionarily impervious to mutation. It is likely *chsE1* and *chsE2* arose from a gene duplication event, allowing for the evolutionary loss of the ChsE1 active site. For a homotetrameric or homodimeric ACAD, loss of an active site would result in loss of function. ChsE1 and ChsE2 share only 7% amino acid identity, while at the DNA level, they are 47% identical. We propose that the complex has evolved to increase the binding pocket size to accommodate polycyclic steroid substrates. Further structural analysis is underway to corroborate this hypothesis. Moreover, the distinct differences in protein architecture between *M. tuberculosis* ChsE1−ChsE2 and human ACADs suggest that specific inhibition of the *M. tuberculosis* enzyme may be possible.

It is well established that *chsE1* and *chsE2* are regulated by cholesterol and involved in the cholesterol metabolism of *M.*

dx.doi.org/10.1021/bi4002979 | *Biochemistry* 2013, 52, 2895−2904

tuberculosis. We have previously shown that this enzyme complex is able to bind and turn over steroid substrates. In this work, our experimentally determined specificity constants for 3-oxo-4-pregnene-20-carboxyl-CoA (**1**) and 1β-(2′-propanoyl-CoA)-3aα-H-7aβ-methylhexahydro-4-indanone (**2**) demonstrate that the ChsE1−ChsE2 complex strongly prefers the ring nucleus intact species to the hexahydroindinone species, *in vitro*. This suggests the side chain of cholesterol is fully metabolized prior to aromatization and degradation of the ring system.

Assignment of biochemical function to genes is complicated by the large number of annotated fatty acid oxidation genes in *M. tuberculosis*.[35] It is impossible to assign enzymes to specific biochemical steps in sterol metabolism from sequence data alone. We propose that the heterotetrameric architecture is important for binding sterols and possibly other polycyclic substrates. Our biochemical characterization and bioinformatic analysis of a heteromeric sterol oxidizing ACAD provide information that will be applied to further proper annotation of the *M. tuberculosis* genome.

■ ASSOCIATED CONTENT

Supporting Information

SDS−PAGE of purified proteins (Figure S1), LC−UV−MS analysis of isolated flavin from ChsE1−ChsE2 (Figure S2), and the salt dependence of dehydrogenase activity (Figure S3). This material is available free of charge via the Internet at http://pubs.acs.org.

■ AUTHOR INFORMATION

Corresponding Author

*Department of Chemistry, Stony Brook University, Stony Brook, NY 11794-3400. E-mail: nicole.sampson@stonybrook.edu. Phone: (631) 632-7952.

Funding

This work was supported by the National Institutes of Health (R21AI092455, R01HL53306, and S10RR021008, N.S.S.), National Science Foundation Grant BIO1039771 (NMR), and a DOE-GAANN fellowship (S.T.T.).

Notes

The authors declare no competing financial interest.

■ ACKNOWLEDGMENTS

We thank Francis Picart (NMR Coordinator, Stony Brook University) for his assistance in NMR acquisition.

■ ABBREVIATIONS

ACAD, acyl-CoA dehydrogenase; igr, intracellular growth; IPTG, isopropyl β-D-1-thiogalactopyranoside; HEPES, 4-(2-hydroxyethyl)-1-piperazineethanesulfonic acid; Tris, tris-(hydroxymethyl)aminomethane; IMAC, immobilized metal ion affinity chromatography; TAPS, *N*-tris(hydroxymethyl)-methyl-3-aminopropanesulfonic acid; TCEP, tris(2-carboxyethyl)phosphine; FAD, flavin adenine dinucleotide; AUC, analytical ultracentrifugation; CoA, coenzyme A.

■ REFERENCES

(1) World Health Organization (2011) *Global Tuberculosis Control 2011*.

(2) Russell, D. G., Cardona, P. J., Kim, M. J., Allain, S., and Altare, F. (2009) Foamy macrophages and the progression of the human tuberculosis granuloma. *Nat. Immunol. 10*, 943−948.

(3) Peyron, P., Vaubourgeix, J., Poquet, Y., Levillain, F., Botanch, C., Bardou, F., Daffe, M., Emile, J. F., Marchou, B., Cardona, P. J., de Chastellier, C., and Altare, F. (2008) Foamy macrophages from tuberculous patients' granulomas constitute a nutrient-rich reservoir for *M. tuberculosis* persistence. *PLoS Pathog. 4*, e1000204.

(4) Pandey, A. K., and Sassetti, C. M. (2008) Mycobacterial persistence requires the utilization of host cholesterol. *Proc. Natl. Acad. Sci. U.S.A. 105*, 4376−4380.

(5) Mohn, W. W., van der Geize, R., Stewart, G. R., Okamoto, S., Liu, J., Dijkhuizen, L., and Eltis, L. D. (2008) The actinobacterial mce4 locus encodes a steroid transporter. *J. Biol. Chem. 283*, 35368−35374.

(6) Nesbitt, N., Yang, X., Fontán, P., Kolesnikova, I., Smith, I., Sampson, N. S., and Dubnau, E. (2010) A thiolase of *M. tuberculosis* is required for virulence and for production of androstenedione and androstadienedione from cholesterol. *Infect. Immun. 78*, 275−282.

(7) Chang, J. C., Miner, M. D., Pandey, A. K., Gill, W. P., Harik, N. S., Sassetti, C. M., and Sherman, D. R. (2009) *igr* Genes and *Mycobacterium tuberculosis* cholesterol metabolism. *J. Bacteriol. 191*, 5232−5239.

(8) Chang, J. C., Harik, N. S., Liao, R. P., and Sherman, D. R. (2007) Identification of Mycobacterial genes that alter growth and pathology in macrophages and in mice. *J. Infect. Dis. 196*, 788−795.

(9) Thomas, S. T., VanderVen, B. C., Sherman, D. R., Russell, D. G., and Sampson, N. S. (2011) Pathway profiling in *Mycobacterium tuberculosis*: Elucidation of cholesterol-derived catabolite and enzymes that catalyze its metabolism. *J. Biol. Chem. 286*, 43668−43678.

(10) Zhang, J., Zhang, W., Zou, D., Chen, G., Wan, T., Zhang, M., and Cao, X. (2002) Cloning and functional characterization of ACAD-9, a novel member of human acyl-CoA dehydrogenase family. *Biochem. Biophys. Res. Commun. 297*, 1033−1042.

(11) Souri, M., Aoyama, T., Hoganson, G., and Hashimoto, T. (1998) Very-long-chain acyl-CoA dehydrogenase subunit assembles to the dimer form on mitochondrial inner membrane. *FEBS Lett. 426*, 187−190.

(12) Moore, S. (2012) 'Round-the-horn site-directed mutagenesis. *Wikiomics*.

(13) Daugelat, S., Kowall, J., Mattow, J., Bumann, D., Winter, R., Hurwitz, R., and Kaufmann, S. H. (2003) The RD1 proteins of *Mycobacterium tuberculosis*: Expression in *Mycobacterium smegmatis* and biochemical characterization. *Microbes Infect. 5*, 1082−1095.

(14) Shevchenko, A., Tomas, H., Havlis, J., Olsen, J. V., and Mann, M. (2006) In-gel digestion for mass spectrometric characterization of proteins and proteomes. *Nat. Protoc. 1*, 2856−2860.

(15) Winkler, R. (2010) ESIprot: A universal tool for charge state determination and molecular weight calculation of proteins from electrospray ionization mass spectrometry data. *Rapid Commun. Mass Spectrom. 24*, 285−294.

(16) Thompson, J. D., Higgins, D. G., and Gibson, T. J. (1994) CLUSTAL W: Improving the sensitivity of progressive multiple sequence alignment through sequence weighting, position specific gap penalties and weight matrix choice. *Nucleic Acids Res. 22*, 4673−4680.

(17) Stierand, K., Maass, P. C., and Rarey, M. (2006) Molecular complexes at a glance: Automated generation of two-dimensional complex diagrams. *Bioinformatics 22*, 1710−1716.

(18) Capyk, J. K., Casabon, I., Gruninger, R., Strynadka, N. C., and Eltis, L. D. (2011) Activity of 3-ketosteroid 9α-hydroxylase (KshAB) indicates cholesterol side chain and ring degradation occur simultaneously in *Mycobacterium tuberculosis*. *J. Biol. Chem. 286*, 40717−40724.

(19) Lehman, T. C., and Thorpe, C. (1990) Alternate electron acceptors for medium-chain acyl-CoA dehydrogenase: Use of ferricenium salts. *Biochemistry 29*, 10594−10602.

(20) Ellis, K. J., and Morrison, J. F. (1982) Buffers of constant ionic strength for studying pH-dependent processes. *Methods Enzymol. 87*, 405−426.

(21) Hwang, T. L., and Shaka, A. J. (1995) Water suppression that works: Excitation sculpting using arbitrary wave-forms and pulsed-field gradients. *J. Magn. Reson., Ser. A 112*, 275−279.

(22) Djordjevic, S., Dong, Y., Paschke, R., Frerman, F. E., Strauss, A. W., and Kim, J. J. (1994) Identification of the catalytic base in long chain acyl-CoA dehydrogenase. *Biochemistry 33*, 4258−4264.
(23) Sih, C. J., Tai, H. H., and Tsong, Y. Y. (1967) The mechanism of microbial conversion of cholesterol into 17-keto steroids. *J. Am. Chem. Soc. 89*, 1957−1958.
(24) Sih, C. J., Tai, H. H., Tsong, Y. Y., Lee, S. S., and Coombe, R. G. (1968) Mechanisms of steroid oxidation by microorganisms. XIV. Pathway of cholesterol side-chain degradation. *Biochemistry 7*, 808−818.
(25) Sih, C. J., Wang, K. C., and Tai, H. H. (1968) Mechanisms of steroid oxidation by microorganisms. XIII. C22 acid intermediates in degradation of cholesterol side chain. *Biochemistry 7*, 796−807.
(26) Bode, K., Hooks, M. A., and Couee, I. I. (1999) Identification, separation, and characterization of acyl-coenzyme A dehydrogenases involved in mitochondrial β-oxidation in higher plants. *Plant Physiol. 119*, 1305−1314.
(27) Komuniecki, R., Fekete, S., and Thissen-Parra, J. (1985) Purification and characterization of the 2-methyl branched-chain Acyl-CoA dehydrogenase, an enzyme involved in NADH-dependent enoyl-CoA reduction in anaerobic mitochondria of the nematode, *Ascaris suum*. *J. Biol. Chem. 260*, 4770−4777.
(28) Kionka, C., and Kunau, W. H. (1985) Inducible β-oxidation pathway in *Neurospora crassa*. *J. Bacteriol. 161*, 153−157.
(29) Kunau, W. H., Dommes, V., and Schulz, H. (1995) β-Oxidation of fatty acids in mitochondria, peroxisomes, and bacteria: A century of continued progress. *Prog. Lipid Res. 34*, 267−342.
(30) Campbell, J. W., and Cronan, J. E., Jr. (2002) The enigmatic *Escherichia coli* fadE gene is yafH. *J. Bacteriol. 184*, 3759−3764.
(31) Shen, Y. Q., Lang, B. F., and Burger, G. (2009) Diversity and dispersal of a ubiquitous protein family: Acyl-CoA dehydrogenases. *Nucleic Acids Res. 37*, 5619−5631.
(32) Swigonova, Z., Mohsen, A. W., and Vockley, J. (2009) Acyl-CoA dehydrogenases: Dynamic history of protein family evolution. *J. Mol. Evol. 69*, 176−193.
(33) McAndrew, R. P., Wang, Y., Mohsen, A. W., He, M., Vockley, J., and Kim, J. J. (2008) Structural basis for substrate fatty acyl chain specificity: Crystal structure of human very-long-chain acyl-CoA dehydrogenase. *J. Biol. Chem. 283*, 9435−9443.
(34) Hiltunen, J. K., and Qin, Y. (2000) β-Oxidation: Strategies for the metabolism of a wide variety of acyl-CoA esters. *Biochim. Biophys. Acta 1484*, 117−128.
(35) Cole, S. T., Brosch, R., Parkhil, J., Garnier, T., Churcher, C., Harris, D., Gordon, S. V., Eiglmeier, K., Gas, S., Barry, C. E., III, Tekaia, F., Badcock, K., Basham, D., Brown, D., Chillingworth, T., Connor, R., Davies, R., Devlin, K., Feltwell, T., Gentles, S., Hamlin, N., Holroyd, S., Hornsby, T., Jagels, K., Krogh, A., McLean, J., Moule, S., Murphy, L., Oliver, K., Osborne, J., Quail, M. A., Rajandream, M. A., Rogers, J., Rutter, S., Seeger, K., Skelton, J., Squares, R., Squares, S., Sulston, J. E., Taylor, K., Whitehead, S., and Barrell, B. G. (1998) Deciphering the biology of *Mycobacterium tuberculosis* from the complete genome sequence. *Nature 393*, 537−544.